Journal of the Indian Institute of Science
A Multidisciplinary Reviews Journal
ISSN: 0970-4140 Coden-JIISAD

REVIEWS

Frustration in Optical Lattices of Interacting Bosons

Subroto Mukerjee

Abstract | The realization of optical lattices of cold atoms has opened up the possibility of engineering interacting lattice systems of bosons and fermions, stimulating a frenzy of research over the last decade. More recently, experimental techniques have been developed to apply synthetic gauge fields to these optical lattices. As a result, it has become possible to study quantum Hall physics and the effects of frustration in lattices of cold atoms. In this article we describe the combined effect of frustration and interactions on the superfluidity of bosons. By focussing on a frustrated ladder of interacting bosons, we show that the effect of frustration is for "chiral" order to develop, which manifests itself as an alternating pattern of circulating supercurrents. Remarkably, this order persists even when superfluidity is lost and the system enters a Mott phase giving rise to a novel chiral Mott insulator. We describe the combined physics of frustration and interactions by studying a fully frustrated one dimensional model of interacting bosons. The model is studied using mean-field theory, a direct quantum simulation and a higher dimensional classical theory in order to offer a full description of the different quantum phases contained in it and transitions between the different phases. In addition, we provide physical descriptions of the chiral Mott insulator as a vortex-anitvortex super solid and indirect excitonic condensate in addition to obtaining a variational wavefunction for it. We also briefly describe the chiral Mott states arising in other microscopic models.

1 Introduction

Over the last two decades, several technical advances in the field of trapping and cooling of ultra-cold atoms has made it possible to study the collective behaviour of bosons, fermions and their mixtures. Pioneering experimental work in this field led to the realisation of a Bose-Einstein-Condensate (BEC) in a system of ^{87}Rb atoms.[1,2] Associated with the phenomenon of Bose-Einstein Condensation is the related phenomenon of superfluidity, where a fluid of particles flows with no viscosity. While ^{4}He at very low temperatures (<2.7 K) is known to be a superfluid, its relatively high density makes it quite different from the idealized non-interacting BEC predicted by Einstein building on the work of Bose.[3–5] A BEC of cold alkali atoms, which is at much lower densities than ^{4}He is a much better approximation to the idealized BEC. More recently, BECs of bosons with non-zero spin have also been realized which have made it possible to investigate a combination of superfluid and magnetic behavior.[6] Almost a decade later, using ^{87}Rb atoms, a condensate of fermionic pairs was realized in a system of ^{40}K atoms.[7] The fermionic atoms of ^{40}K pair up like in a superconductor due to an attractive interaction among them. An area of intense activity is the study of the dynamics of pairing in such fermionic systems, especially the transition from having a superfluid of weakly attracting fermions (the so-called BCS state) to one where a strong attraction causes the fermions to pair up first and then condense (the so-called BEC state).[8]

The realization of many body bosonic and fermionic states in systems of cold atoms opens up the possibility of using them to emulate such states found in solid state systems. An advantage afforded by cold atomic systems is the tunability of

Department of Physics, Indian Institute of Science, Bangalore 560012, India.

microscopic parameters, which is often extremely difficult in actual solid systems; another is the elimination of effects of disorder and phonons, which might hinder the study of the effects of correlations among the bosons and fermions. Real solid systems typically exist on lattices and have correlations among the elementary degrees of freedom such as in magnets and superconductors (for fermions) or Josephson junction arrays (for bosons). A phase transition from a superfluid to an insulating Mott state had been predicted theoretically for Josephson junction arrays[9] which was observed by Greiner *et al.* in an important experiment, in a system of cold atoms trapped to form an optical lattice.[10] This observation sparked off a rush of experimental and theoretical work over the last decade aimed at studying the effect of correlations in lattice systems of cold atoms.[11,12]

An important technological development over the last few years has been the ability to apply synthetic gauge fields to lattice systems of ultra-cold atoms.[13] The alkali atoms that are used in conventional cold atom experiments are electrically neutral, and hence their orbital degrees of freedom do not couple to ordinary magnetic fields. However, exploiting the physics of Raman transitions in the alkali atoms has enabled the production of synthetic gauge fields that couple to orbital degrees of freedom, mimicking the effect of a magnetic field on a gas of ^{87}Rb atoms.[14,15] Artificial magnetic fields have also been applied to optical lattices of cold atoms in a variety of different ways. These include applying homogeneous[16] and inhomogeneous fluxes,[17,18] Zeeman techniques,[19] and driving the optical lattice with a time dependent potential.[20,21] The interplay of lattice effects and magnetic fields gives rise to very interesting physics such as that of the Hofstadter butterfly and the quantum Hall effect in lattice systems.[22] Moreover, the technique of generating artificial gauge fields can also be extended to produce spin-orbit coupling[23–27] which is known to be responsible for producing novel states of matter such as the topological insulator in solid state systems.[28–30] The spin hall effect has been observed in cold atomic systems.[31]

Artificial gauge fields can be used to thread fluxes through the plaquettes of optical lattices. For the right values of the flux, this can introduce "kinetic frustration" producing degenerate multiple minima in the band structure. If bosons had to condense in such a landscape, the multiple minima would frustrate condensation into a single minimum. Any superfluid state thus formed, would in addition to breaking gauge symmetry, (which is responsible for superfluidity) also break a discrete symmetry corresponding to the choice of minimum (or a particular linear combination) to condense in. This has been demonstrated in the case of weak repulsive interactions among the bosons.[32–36] A natural question to ask is, as to what happens when the strength of the repulsion increases. For a very large repulsion, it can be argued that a regular Mott insulator (MI) develops, which does not break any symmetries. However, at intermediate strength it has been argued that, for maximum frustration, a novel Chiral Mott Insulator (CMI) state that has no superfluidity develops, but breaks the discrete symmetry arising from frustration.[37–41] An example of a lattice that is maximally frustrated is one with square plaquettes and a flux equal to π per plaquette. When repulsive on site interactions are added to such a lattice for bosons, the model obtained is the Fully Frustrated Bose Hubbard (FFBH) model. The chiral order that develops due to the frustration manifests itself as an alternating pattern of clockwise and anti-clockwise currents on neighboring plaquettes. The superfluid obtained at weak interaction strength also possesses this order, and is thus a Chiral Superfluid (CSF).

Classical analogues of the FFBH have been studied in the past.[42–45] The simplest example of such a model is the fully frustrated XY model, which displays three phases: a low temperature phase which corresponds to in-plane magnetic order and a staggered chirality of the spins in adjacent plaquettes, an intermediate phase where the chirality remains but the in-plane order is lost, and finally a high temperature phase which is fully disordered. These phase are the analogues of the CSF, CMI and MI respectively.

In this article, we describe the physics of chiral states in the interacting bosonic systems by focussing a specific model, a one dimensional fully frustrated square ladder. We first describe the Hamiltonian of the model and the phases it is expected to contain. We then provide a mean field description of the Hamiltonian, which provides the simplest description of the CSF phase and the phase transition out of it. It will be seen that at the mean-field level, the exist. To capture the CMI, quantum fluctuations that are absent in the mean-field description have to be included. This will be done in two ways: 1) by simulating the quantum mechanical system directly using the Density Matrix Renormalization Group (DMRG) algorithm, and 2) by mapping the Hamiltonian onto a higher dimensional classical model and then performing Monte-Carlo simulations on that model. Both of these techniques will allow a clear description of all the phases contained in the model (most

importantly the CMI) and the transitions between them. We will then provide physical pictures for the CMI, as a vortex-antivortex supersolid and an indirect excitonic condensate, and also furnish a variational wavefunction that describes it. We will conclude with a brief description of the CMI phase in other bosonic systems.

2 Hamiltonian and Phases

The system of interacting bosons on a ladder with a frustrating π flux per plaquette is shown in Fig. 1. The microscopic Hamiltonian for such a system (which we call the fully frustrated Bose-Hubbard ladder) is

$$\begin{aligned} H = & -t\sum_x (a_x^\dagger a_{x+1} + a_{x+1}^\dagger a_x) \\ & + t\sum_x (b_x^\dagger b_{x+1} + b_{x+1}^\dagger b_x) \\ & - t_\perp \sum_x (a_x^\dagger b_x + b_x^\dagger a_x) \\ & + \frac{U}{2}\sum_x (n_{a,x}^2 + n_{b,x}^2) \end{aligned} \quad (1)$$

where a_x and b_x are bosonic operators on each of the two legs of the ladder whose sites are labeled by x. The hopping amplitudes along the two legs are t and $-t$, while $t_\perp$ is the amplitude along the rungs.[37,38] U is the on-site repulsion. The opposite signs of the hopping amplitude along the two legs provides the π flux that fully frustrates the ladder. However, it should be noted that this corresponds to a particular choice of gauge. Another gauge choice is one in which the hopping amplitude is the same along both legs but $t_\perp$ alternates in sign from rung to rung. The phases and phase transitions we describe are characterized by gauge independent quantities, and so we pick the most convenient gauge for us to work in, which is the one described above. We analyze the system at a filling of one boson per site in order to study both superfluid and Mott phases.

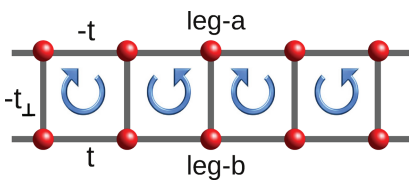

Figure 1: The fully frustrated Bose-Hubbard ladder. The hopping is equal and opposite on the two legs *a* and *b* legs generating a π-flux through each plaquette. This gives rise to spontaneously generated staggered loop currents that are also shown.

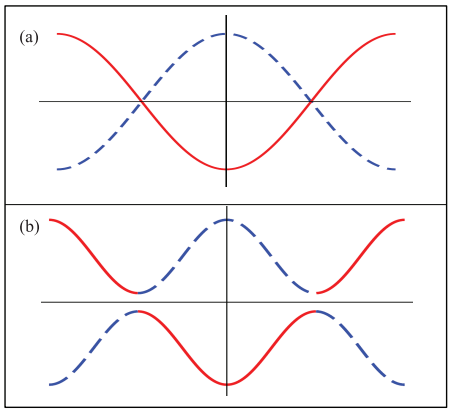

Figure 2: (Top) The band structure obtained in Eqn. 1 with $U = 0$ and $t_\perp = 0$. For $t > 0$, the lower (upper) band corresponds to the *a* (*b*) leg as is shown by the solid (dashed) line. (Bottom) For $t_\perp \neq 0$, the degeneracies at $k = \pm\pi/2$ are lifted resulting in a gap and two minima. The $k = 0$ (π) minimum originates from the lower (upper) band of the two decoupled chains, and thus corresponds to the particles being localized mostly in the *a* (*b*) legs.

To understand the superfluid phase, we look at Eqn. 1 with $U = 0$. The band structure thus obtained can be understood systematically in the following way: If $t_\perp = 0$, the two legs are decoupled and give rise to the two bands shown in the top panel of Fig. 2 which are degenerate at $k = \pm\pi/2$. $t_\perp \neq 0$ lifts this degeneracy yielding the band structure shown in the bottom panel of Fig. 2. There are now two minima at $k = 0$ and $k = \pi$, which correspond to the particles being mostly on the *a* and *b* legs. The occurrence of these two minima is a consequence of the frustration in the system.

The most general superfluid state that can be obtained for bosons with the above dispersion is one in which they condense in a state which has the general form[a]

$$|\psi\rangle = A|k = 0\rangle + B|k = \pi\rangle$$

The mean occupancies of the two legs are proportional to $|A|^2$ and $|B|^2$. Switching on U disfavours double occupancy. Since the filling is one boson per site, this implies that $|A| = |B|$ and thus the wavefunction has the form

$$|\psi\rangle = |A|e^{i\theta}\left(|k = 0\rangle + e^{i\phi}|k = \pi\rangle\right) \quad (2)$$

where θ is the global phase and ϕ, the relative phase between the states corresponding to the two

[a] Since this is a one dimensional system, only a quasi-condensate is formed.

minima. As will be shown below, $\phi = \pm\pi/2$, implying that a $U(1) \times Z_2$ symmetry is broken in the superfluid state with $U(1)$ corresponding to θ and Z_2 to ϕ. Since this a one dimensional system, the $U(1)$ order is quasi-long-ranged while the Z_2 order is truly long-ranged. The Z_2 Ising degree of freedom corresponds to the pattern of staggered currents shown in Fig. 1. Thus, the superfluid state is one in which there is "chiral" pattern of supercurrents and is the Chiral Superfluid (CSF). Increasing U leads to a localization of the bosons resulting in a Mott insulator.[9] However, in contrast to the regular Mott transition in interacting Bose systems, this system of frustrated bosons undergoes two transitions, one each corresponding to restoring the $U(1)$ and Z_2 symmetries. The situation here is reminiscent of classical two dimensional fully frustrated XY systems, which too have a low temperature phase with quasi-long-ranged $U(1)$ order and true long-ranged Ising order.[42] As the temperature is increased, the $U(1)$ symmetry is first restored followed by the Z_2 symmetry via Berezinski-Kosterlitz-Thouless (BKT) and 2D Ising transitions respectively.[46] We will make this analogy of the frustrated system of bosons with the classical two dimensional system more concrete, and show that the former too undergoes the same sequence of transitions.

For our system, the phase that is obtained after both symmetries has been restored is the regular Mott insulator, seen in more conventional systems of interacting bosons.[10] However, the intermediate phase, which corresponds to the $U(1)$ symmetry being restored but the Z_2 symmetry broken is a new kind of insulating phase, which has a staggered pattern of currents. This is the Chiral Mott Insulator (CMI), and as we will argue, can be thought of as a vortex-antivortex supersolid or an indirect excitonic condensate. Thus, the fully frustrated ladder of interacting bosons has three phases—the chiral superfluid, the chiral Mott insulator and the Mott insulator.

3 Mean-Field Theory

The simplest way to understand the CSF state is through a mean-field analysis of the Hamiltonian of Eqn. 1. It can be shown that the low energy mean-field theory describing the system is of the form

$$\begin{aligned} E^{\text{mft}}_{\text{low}} = {} & (-E_0 - \mu) \sum_{i=0,\pi} |\varphi_i|^2 \\ & + U(u_0^4 + v_0^4) \sum_{i=0,\pi} |\varphi_i|^4 \\ & + 8Uu_0^2 v_0^2 |\varphi_0|^2 |\varphi_\pi|^2 \\ & + 2Uu_0^2 v_0^2 (\varphi_0^{*2}\varphi_\pi^2 + \varphi_\pi^{*2}\varphi_0^2) \end{aligned} \tag{3}$$

where φ_i is the amplitude to condense bosons in the $i = 0$ or π minimum.[38] μ is the chemical potential and

$$u_k = \frac{1}{\sqrt{1+g_k^2}} = \sqrt{\frac{1}{2}\left(1 + \frac{2t\cos k}{E_k}\right)} \tag{4}$$

$$v_k = \frac{g_k}{\sqrt{1+g_k^2}} = \sqrt{\frac{1}{2}\left(1 - \frac{2t\cos k}{E_k}\right)} \tag{5}$$

$$u_k v_k = \frac{t_\perp}{2E_k} \tag{6}$$

where $g_k = (E_k - 2t)/t_\perp$ with

$$E_k = \sqrt{t_\perp^2 + (2t\cos k)^2} \tag{7}$$

the single boson dispersion. It should be noted that $u_{k+\pi} = v_k$ and $v_{k+\pi} = u_k$, so that in particular $u_\pi = v_0$ and $v_\pi = u_0$, which are the quantities that appear in Eqn. 3. Minimizing the energy in Eqn. 3 with respect to φ_i gives $|\varphi_0| = |\varphi_\pi|$, and the phase difference between the two amplitudes equal to $\pm\pi/2$. The latter is a consequence of the last umklapp term on the right-hand side of Eqn. 3. It can be shown that the superfluid state thus described has bond currents of the form

$$\begin{aligned} j^a_{x,x+1} &= \mp 4t\psi^2 u_0 v_0 (-1)^x \\ j^b_{x,x+1} &= \pm 4t\psi^2 u_0 v_0 (-1)^x \\ j^{ab}_x &= \mp 2t_\perp \psi^2 (u_0^2 - v_0^2)(-1)^x \end{aligned} \tag{8}$$

where $j^{a(b)}_{x,x+1}$ is the current along a bond between sites x and $x+1$ along the $a(b)$ leg, and j^{ab}_x is the current along the rung situated at x. It can be seen from the forms of these currents that they correspond exactly to the pattern of currents shown in Fig. 1 and also that current is conserved at each vertex.

A single-site mean field analysis of the Hamiltonian of Eqn. 1 allows us to study the Mott phase. It can be shown that such an analysis yields only a single transition from the CSF to the MI with a phase boundary for the nth Mott lobe given by

$$\frac{1}{\sqrt{4t^2 + t_\perp^2}} = \frac{n}{\mu - U(n-1)} + \frac{n+1}{Un - \mu} \tag{9}$$

with $U(n-1) < \mu < Un$.[38] Thus, the CMI phase is a product of quantum fluctuations not captured by a single-site mean field theory and requires other techniques for its analysis. We describe two

such techniques below which are a) a Density Matrix Renormalization Group (DMRG) study of the Hamiltonian of Eqn. 1 and b) a Monte-Carlo simulation of an equivalent classical two dimensional system.

4 DMRG Calculations

DMRG is a technique that is most suited for the determination of the ground state of a one dimensional Hamiltonian, and is based on the matrix product representation of the state.[47,48] DMRG calculations for the Hamiltonian of Eqn. 1 have been performed for systems up to 200 sites with the occupancy restricted to 6 bosons per site.[37] Further, up to 200 terms were retained in the matrix product representation. The different phases were characterized by calculating the occupancy of the $k = 0$ state, $n(k = 0)$ and the current-current structure factor

$$S_j(k) = \frac{1}{L^2} \sum_{x,x'} e^{ik(x-x')} \langle j_x j_{x'} \rangle \qquad (10)$$

where the current $j_x = i\left(a_x^\dagger b_x - b_x^\dagger a_x\right)$. Staggered current ordering corresponds to a non-zero structure factor at $k = \pi$, which can be regarded as the order parameter for this type of ordering.

The transition from the CSF to CMI phase is of the BKT type as can be seen from the characteristic BKT finite-size scaling of $n(k = 0)$ in Fig. 4. At the transition, a charge gap opens up going into the CMI phase even as $S(k = \pi)$ remains non-zero and continuous since both phases have chiral order. This concurrent opening of a charge gap at the transition determined from the BKT scaling can also be seen in Fig. 3.

The transition from the CMI to the MI phase corresponds to the disappearance of chiral order. The relevant order parameter to detect this transition is thus $S(k = \pi)$. Appropriate scaling plots of $S(k = \pi)$ are shown in Fig. 3, where it can be seen that a sharp transition is obtained when the relevant critical exponents are of the 2D Ising universality class. It should be noted that the scaling analysis to obtain each of the two transitions is different since the CSF phase only has algebraically long-ranged superfluid order while the CMI phase has true long-ranged chiral order.

On the basis of the DMRG calculations, we can obtain the phase diagram shown in Fig. 4. It can be seen that while the two transitions are quite close to each other in the parameter space of the Hamiltonian of Eqn. 1, they clearly mark out a sliver of the CMI phase separating the CSF and the CMI phase.

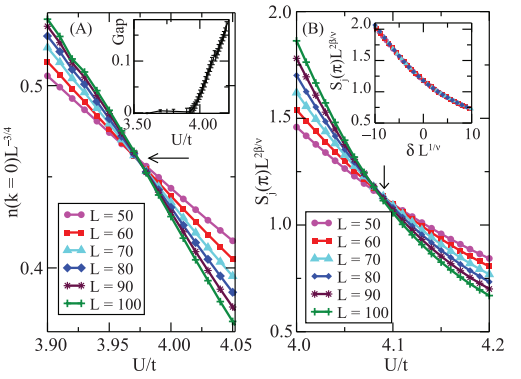

Figure 3: From Ref 37. (A) DMRG results for $n(k = 0)L^{-3/4}$ versus U/t, for the Hamiltonian in Eqn. 1 with $t_\perp = t$ and various L. The crossing of these curves at a particular value of U_{c1}/t is indicative of a BKT transition from the CSF to CMI phase. The inset shows the onset of the charge gap at U_{c1}/t. (B) The structure factor $S_j(k = \pi)L^{2\beta/\nu}$ versus U/t for different L with $t_\perp = t$ where $\beta = 1/8$ and $\nu = 1$ are the order parameter and correlation length critical exponents of the 2D Ising universality class. The intersection of these curves at a point U_{c2}/t indicates a transition from the CMI to MI in the 2D Ising universality class. The inset shows $S_j(k = \pi)L^{2\beta/\nu}$ versus $\delta L^{1/\nu}$ with $\delta \equiv (U - U_{c2})/t$, plotted for different U/t, leading to a scaling collapse.

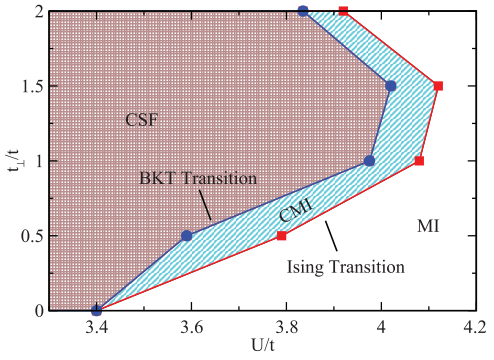

Figure 4: From Ref 37. Phase diagram of the Hamiltonian in Eqn. 1 obtained using DMRG. A sliver of CMI can be seen in parameter space separating the CSF and MI phases.

5 Classical 2D Model

In this section we make the connection of our system to classical 2D XY type systems, alluded to earlier, clearer. Our starting point is a representation of the bosons in terms of quantum rotor fields. We set $a_x \sim e^{-i\varphi_x^a}$ and $b_x \sim e^{-i\varphi_x^b}$, where $\phi_x^{a(b)}$ is the rotor field corresponding to the leg $a(b)$. The

number operators $n^{a,b}$ are replaced by the angular momentum operators $\frac{\partial}{\partial\varphi^{(a,b)}}$. The quantum propagator of the system can now be obtained in terms of a classical action in one higher dimension given by

$$\begin{aligned} S_{\mathrm{cl}}^{1+1} = -\sum_{x\tau} \big[& J_{\parallel} \cos(\varphi^a_{x+1,\tau} - \varphi^a_{x,\tau}) \\ & - J_{\parallel} \cos(\varphi^b_{x+1,\tau} - \varphi^b_{x,\tau}) \\ & + J_{\perp} \cos(\varphi^a_{x,\tau} - \varphi^b_{x,\tau}) \big] \\ - J_{\tau} \sum_{x\tau} \big[& \cos(\varphi^a_{x,\tau+1} - \varphi^a_{x,\tau}) \\ & + \cos(\varphi^b_{x,\tau+1} - \varphi^b_{x,\tau}) \big] \end{aligned} \tag{11}$$

where $2\epsilon = \mathrm{J}_{\|}$, $2\epsilon_{\perp} = \mathrm{J}_{\perp}$, and $1/\epsilon U = J_{\tau}$ with ϵ being the discretization in the extra (imaginary time) dimension.[38] τ labels the imaginary time coordinate. It should be noted that ϵ is not just a simple multiplicative constant and thus the quantum model does not have a unique classical counterpart; there is a different classical model for each value of ϵ. Nevertheless, all of these models are in the same universality class and will display the same phases and phase transitions.

Monte-Carlo simulations have been performed for the action in Eqn. 11.[38] It can be seen that this action has three parameters $J_{\|}$, $J_{\perp}$ and J_{τ} as opposed to the two parameters U/t and $t_{\perp}/t$ of the Hamiltonian of Eqn. 1 reflecting the appearance of the parameter ϵ. Monte-Carlo simulations results with $J_{\|} = J_{\tau}$ and $J_{\perp} = 1$ are shown in Fig. 5.

The CSF phase in this model has quasi-long range order in the variables φ and staggered currents in the plaquettes perpendicular to the imaginary time direction. The CMI phase has only the staggered current order while the MI phase is completely disordered. The CSF-CMI transition is thus of the BKT characterized by the disappearance of the phase stiffness or helicity modulus Γ associated with the variable φ. Formally,

$$\Gamma = \frac{1}{2}\frac{\partial^2 F}{\partial \Phi^2}\bigg|_{\Phi\to 0} \tag{12}$$

where the free energy

$$F = -\log \sum_{\{\varphi_{x,\tau}\}} e^{-S_{\mathrm{cl}}^{1+1}} \tag{13}$$

and Φ is the flux twist along the $\|$ direction. A plot of Γ as a function of $1/J_{\tau}$ is shown in Fig. 5 and it can be seen that there is indeed a BKT transition accompanied by a jump in Γ that gets sharper with increasing system size approaching its thermodynamic limit value of $2/\pi$. The inset shows the RMS error of a fit to a finite-sized scaling form for $\Gamma(L)$

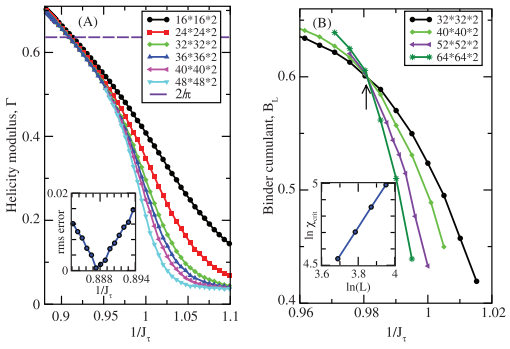

Figure 5: From Ref 37. (A) Helicity modulus Γ versus $1/J_{\tau}$ for different system sizes for $J_{\perp} = 1$ and $J_{\|} = J_{\tau}$. (A-Inset) RMS error of fit to the BKT finite size scaling form of Γ enables a precise determination of the transition at the transition and jump $\Delta\Gamma \approx 0.637$, close to the BKT value of $2/\pi$. (B) Binder cumulants for the staggered current versus $1/J_{\tau}$ (for different L for $J_{\perp} = 1$) intersect showing a continuous transition. (B-inset) Critical susceptibility versus L gives the ratio of critical exponents $\gamma/\nu \approx 1.72$, very close to 2D Ising value $\gamma/\nu = 7/4$.

whose minimum lets us detect the transition more clearly.[49]

The method of Binder cumulants[50] is most suited to detect the transition from the CMI to the MI since the former has true long range order. For an order parameter m, the Binder cumulant is defined as

$$B_L = \left(1 - \frac{\langle m^4\rangle_L}{3\langle m^2\rangle_L^2}\right) \tag{14}$$

where L is the system size. The staggered current order parameter is given by

$$m = \frac{1}{L^2}\sum_{i\tau} (-1)^i J_{i\tau} \tag{15}$$

where $J_{i\tau}$ is the current around a plaquette normal to the time direction. i and τ label the coordinates in the $\|$ and time directions. If $a(i,\tau)$, $a(i+1,\tau)$, $b(i+1,\tau)$ and $b(i,\tau)$ are the vertices of the plaquette going around clockwise, then

$$\begin{aligned} J_{i\tau} = J_{\|} \big[& \sin\left(\varphi^a_{i+1,\tau} - \varphi^a_{i,\tau}\right) \\ & + \sin\left(\varphi^b_{i,\tau} - \varphi^b_{i+1,\tau}\right)\big] \\ + J_{\perp} \big[& \sin\left(\varphi^b_{i+1,\tau} - \varphi^a_{i+1,\tau}\right) \\ & + \sin\left(\varphi^a_{i,\tau} - \varphi^b_{i,\tau}\right)\big] \end{aligned} \tag{16}$$

m is an Ising type order parameter since the current in a plaquette can be clockwise or counterclockwise. Curves of B_L for different L as a

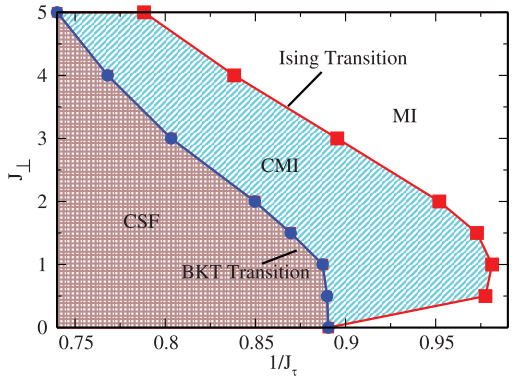

Figure 6: From Ref. 37. Phase diagram for the action in Eqn. 11 with $J_{||} = J_\tau$ obtained from Monte-Carlo simulations. The three phases CSF, CMI and MI can be clearly seen and the transition from the CSF to CMI phase is of the BKT type while from the CMI to the MI is of the Ising type.

function of the tuning parameter intersect at the transition, and this intersection point can be used to find the precise location of the transition. An advantage of this method is that the detection of the transition does not require any knowledge of its universality class, only that the ordered state has long range order. Plots of the Binder cumulant are shown in Fig. 5, from which it can be clearly seen that there is a transition at which staggered current order disappears. Having located the transition this way, it is confirmed to be in the 2D Ising universality class by plotting the critical susceptibility as a function of system size, yielding the right value for the exponent γ/ν.

The phase diagram obtained from these Monte-Carlo simulations is shown in Fig. 6. As in Fig. 4, it can be seen that there is a region of the CMI sandwiched between the CSF and the MI phases. It should be noted that the size and shape of the region of the CMI in parameter space in Fig. 6 is different from that in Fig. 4. This is because, as mentioned earlier, the classical action in Eqn. 11 does not uniquely correspond to the quantum Hamiltonian Eqn. 1, requiring an additional parameter ϵ. However, as expected the phases and phase transitions are the same for the two models.

6 Physical Pictures of the CMI

As seen from the above analysis, the CMI phase is an interesting new phase with a charge gap and staggered currents (chiral order). Two physical descriptions are of this phase as a) a vortex-antivortex supersolid and b) an indirect excitonic condensate.[38]

6.1 *Vortex-antivortex supersolid*

We first start with the CSF, which in the absence of quantum fluctuations can be thought of as a perfect vortex-antivortex crystal since such a crystal has the required long-ranged staggered current order. On the other hand, the MI without quantum fluctuations can be thought of as a superfluid with perfectly mobile vortices and antivortices which destroy superfluid order and introduce a charge gap. An intermediate situation can be envisaged in which the vortex-antivortex solid develops a small number of coherent defects which can move about destroying the superfluidity but still maintaining the chiral order. This resulting phase, which can be thought of as a vortex-antivortex supersolid, is the CMI. From the above discussion, it is clear that the transition from vortex-antivortex solid (CSF) to vortex-antivortex supersolid (CMI) to vortex-antivortex superfluid (MI) happens as a function of increasing interaction strength.

6.2 *Indirect excitonic condensate*

A more quantitative picture of the CMI is afforded by thinking of it as an indirect excitonic condensate. In this picture, the CMI is approached from the MI phase. The excitations of the Mott phase are states of double occupancy (doublons) and zero occupancy (holes). These excitations require a finite amount of energy to create since the Mott state is gapped and are mobile and so have a dispersion in momentum k. It can be shown that the dispersion of the doublons and holons $\varepsilon(k)$ is given by

$$\varepsilon(k) = \frac{U}{2} - \left(n_0 + \frac{1}{2}\right) E(k) \qquad (17)$$

where the chemical potential has been adjusted to give the same dispersion for both types of excitations.[38] $E(k)$ is the single particle dispersion given by Eqn. 7. A very crude estimate of the transition from the Mott state to a superfluid state is obtained by setting $\varepsilon(k) = 0$ such that the doublon and holon excitations become gapless. This gives a value of the transition point that is within a factor of 2 of the DMRG result for $t = t_\perp$. This result also suggests that the doublons and holons can be thought of as being like gapped particles and holes in a semiconductor and the Mott transition can be thought of as the metallization of a semiconductor. The semiconductor picture of a Mott insulating state allows us to think of particle-hole bound states analogous to excitons. When the charge gap is small, in the vicinity of the superfluid to Mott transition, it might be favorable to create such excitons. Since the dispersion $E(k)$

has two minima (at $k = 0$ and $k = \pi$), the excitons thus created can be direct or indirect. It can be shown that the rung current operator in the Mott phase can be written as

$$j_{ab}(x)|\text{Mott}\rangle = -it_{\perp}\sqrt{n_0(n_0+1)}(d_a^{\dagger}(x)h_b^{\dagger}(x) - d_b^{\dagger}(x)h_a^{\dagger}(x))|\text{Mott},\rangle \quad (18)$$

where n_0 is the filling factor and $d_{a(b)}^{\dagger}(x)$ creates a doublon at positon x in leg $a(b)$, while $h_{a(b)}^{\dagger}(x)$ creates a holon at position x in leg $a(b)$.[38] Writing $d_{a(b)}^{\dagger}$ and $h_{a(b)}^{\dagger}$ in momentum space, it can be shown that long range staggered order in j_{ab} can be produced when the composite operator $d_0^{\dagger}h_{\pi}^{\dagger} - h_0^{\dagger}d_{\pi}^{\dagger}$ acquires an expectation value while $d_{0/\pi}^{\dagger}$ and $h_{0/\pi}^{\dagger}$ do not.[38] Here $d_{0/\pi}^{\dagger}$ and $h_{0/\pi}^{\dagger}$ create doublons and holons respectively at $k = 0$ and $k = \pi$. Physically, this corresponds to condensing excitons with the particles and holes at different minima, and thus a picture of the CMI is that of an indirect condensate of excitons. It should be noted that the number of excitations at each minimum can change due to umklapp processes which can scatter a pair of bosons from one valley to another without changing crystal momentum. Thus, the exciton condensate only breaks a discrete Z_2 symmetry associated with the parity of bosons in each valley as opposed to a $U(1)$ symmetry normally associated with condensates.

While the above analysis gives us a physical picture of the CMI, it does not establish that such a state should actually exist. Indeed, an alternative picture could involve a combined presence of holon and doublon modes and such excitons which might render the transition first order.

6.3 *Variational wavefunction*

A wavefunction for the CMI can be constructed starting with the wavefunction for the CSF and multiplying it by appropriate Jastrow factors. Such a wavefunction is of the form

$$\Psi(r_1, r_2, \ldots, r_N) = \mathrm{e}^{-\sum_{i,j}\tilde{v}(r_i - r_j)} \times \Psi_{CSF}(r_1, r_2, \ldots, r_N) \quad (19)$$

where $r_1, r_2, \ldots, r_N$ are the coordinates of the N bosons in the state. The Jastrow factor $\tilde{v}$ is chosen to have an on site (Gutzwiller) piece with strength g_S and a long-ranged piece with Fourier transform $\tilde{v}_{LR}(q) = 1/(1 - \cos q)$ with strength g_L. This choice of $\tilde{v}_{LR}$ produces the $1/q^2$ dependence at small q required for a 1D insulator.[51] The properties of the resultant wavefunction have been studied using Monte-Carlo sampling with 10^6–10^7 boson configurations on a two leg ladder with up to 500 sites. The result of such a sampling for the two point correlator $G^{(2)}(x-x')$ is shown in Fig. 7.

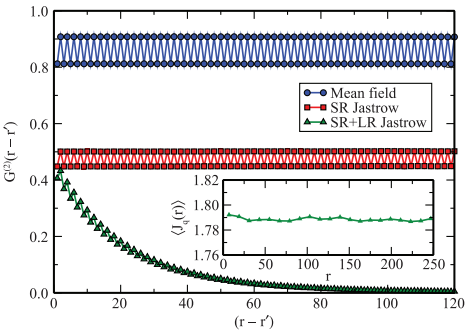

Figure 7: From Ref. 38. The two point correlator $G^{(2)}(x - x') = \langle a_x^{\dagger} a_{x'}\rangle$ computed using variational Monte Carlo method for: (i) the mean field CSF state (circles) with off-diagonal long range order, (ii) a correlated CSF with only an on site Gutzwiller factor (squares), and (iii) the CMI state with an additional long-range Jastrow (triangles) which leads to an exponential decay of $G^{(2)}(x - x')$. The oscillations arise from low energy boson modes at momenta $k = 0$ and $k = \pi$. (Inset) The staggered current order $(-1)^x\langle J_{\square}(x)\rangle$ is non-zero in the mean field CSF and in the CMI.

It can be seen that $G^{(2)}(x - x')$ does not decay in the CSF state as expected, and even the introduction of short range Gutzwiller correlations with $g_S = 1$, while weakening the off-diagonal long range order (and thereby lowering the value of $G^{(2)}(x-x')$) does not destroy superfluidity. It is only upon the introduction of a further long range Jastrow factor with $g_L = 0.1$ that $G^{(2)}(x - x')$ decays exponentially indicating the opening of a gap. The inset of Fig. 7 shows that the staggered current order parameter is indeed non-zero when both g_S and g_L are non-zero. Thus, the state described by the variational wavefunction with short and long ranged Jastrow factors is indeed the CMI.

7 The Chiral Mott Insulator in Other Systems

In the previous sections, we have shown that the CMI develops in the fully frustrated two-leg Bose ladder. A natural question to ask is whether it can be seen in other frustrated lattice models. A natural candidate is a triangular lattice, which was recently studied by Zalatel *et al.*[39] The Hamiltonian they considered was

$$H = \sum_{\langle i,j\rangle}\left[tb_i^{\dagger}b_j + \text{h.c.} + V\delta n_i\delta n_j\right] + \frac{U}{2}\sum_i(\delta n_i)^2 \quad (20)$$

where $\langle i,j\rangle$ labels pairs of nearest-neighbour sites on the triangular lattice and δn_i is the occupancy of site i above an integer filling n_0. $t > 0$ ensures that the band structure is inverted and there are two minima at the Brillouin zone boundaries providing the frustration in this model. Starting with the wavefunction for the MI (which corresponds to an occupancy of exactly n_0 bosons at every site), Zalatel *et al.* documented/presented/derived variational wavefunctions for the CSF and CMI. Minimizing the energy given by Eqn. 20 for each of the three states, they found that the CSF, CMI and MI can all exist within the parameter space of the Hamiltonian. However, a nearest neighbour interaction term with $V > 0$ was required at this mean-field level to obtain the CMI; without the interaction, there is a direct transition from the CSF to the MI like in the mean-field theory for the fully frustrated two-leg Bose ladder. Zalatel *et al.* also performed a DMRG calculation on triangular ladders of up to 4 legs to detect the CMI and a bosonization calculation to argue for the existence of the three phases in these ladders.

A different system in which the CMI phase is seen was studied by Petrescu and Le Hur.[41] They considered a system of two species of interacting bosons capable of inter-conversion and subject to a gauge field. The Hamiltonian describing this system is given by

$$H = -\left[\sum_{\alpha,\langle i,j\rangle} te^{iA_{ij}^{\alpha}} b_{\alpha i}^{\dagger} b_{\alpha j} + ge^{iA_{\perp}{}^{i}} b_{2i}^{\dagger} b_{1j} + \text{h.c.}\right] + V_{\perp}\sum_{i} n_{1i}n_{2i} + \frac{U}{2}\sum_{\alpha i} n_{\alpha i}\left(n_{\alpha i}-1\right) - \mu\sum_{\alpha i} n_{\alpha i} \quad (21)$$

where 1 and 2 label the two species of bosons which can be though to reside on the upper and lower legs of a one dimensional ladder respectively, and $\langle ij\rangle$ represents nearest neighbour sites i and j along a leg of the adder. g is the amplitude for interspecies conversion and V an interaction term for the two species of bosons on the same site which exists in addition to the on-site intra-species interaction U. There exists in addition, a gauge field A which provides a flux χ through each plaquette. Petrescu and Le Hur studied this model using bosonization and exact diagonalization, and obtained the phase diagram for different types of Mott phases (obtained by tuning the chemical potential μ appropriately) as a function of the flux χ. For $\chi = \pi$, the Hamiltonian of Eqn. 21 describes the fully frustrated two leg Bose-Hubbad ladder except for the on-site interaction, and displays a CMI phase. For lower values of flux above a critical value χ_c, flux lattices are obtained with a certain number of plaquettes per unit cell depending on the value of flux as a fraction of 2π. Below χ_c, there is a "Meissner phase" with currents flowing only along the legs (and not the rungs), going one way on the upper leg and the other way along the bottom leg.

8 Conclusions

The combination of frustration and interactions on lattice bosons opens up a window to exciting new physics and novel new phases and transitions. Frustration can be realized by applying synthetic gauge fields which makes it possible to observe and study these phases experimentally. In particular, in this article we have shown that a novel chiral Mott insulator is realized in the fully frustrated two leg Bose-Hubbard ladder. This phase has a charge gap (and hence no superfluidity), but chiral order through a pattern of staggered vortices and antivortice. This phase and the transitions out of it into the chiral superfluid and regular Mott insulator can be described in terms of mean-field theory, a direct quantum simulation using DMRG and mapping onto a higher dimensional classical theory. In addition, physical pictures of the chiral Mott insulator in terms of a vortex-antovortex supersolid and indirect excitonic condensate exist, and the phase can also be described by an appropriate variational wavefunction. The chiral Mott insulator is also realized in triangular ladders and a system of two species of bosons.

Acknowledgments

I would like to thank Arun Paramekanti for a fruitful collaboration on the study of frustrated interacting bosons and many discussions. I would like to thank Ramesh V. Pai for collaborations especially on the DMRG calculations and Tapan Mishra, Maheswar Maji and Arya Dhar for collaborations on many aspects of the calculations described here and other projects. Finally, I would like to thank the Department of Science and Technology, Government of India for support.

Received 17 May 2014.

References

1. M. Anderson, J. Ensher, M. Matthews, C. Wieman, and E. Cornell, Science **269**, 198 (1995).
2. K. Davis, M.-O. Mewes, M.v. Andrews, N. Van Druten, D. Durfee, D. Kurn, and W. Ketterle, Phys. Rev. Lett. **75**, 3969 (1995).
3. S. Bose, Z. Physik **26**, 178 (1924).
4. A. Einstein, Sitzber. Kgl. Preuss. Akad. Wiss. p. 261 (1924).

5. A. Einstein, Sitzber. Kgl. Preuss. Akad. Wiss. p. 3 (1925).
6. D. Stamper-Kurn, M. Andrews, A. Chikkatur, S. Inouye, H.-J. Miesner, J. Stenger, and W. Ketterle, Phys. Rev. Lett. **80**, 2027 (1998).
7. M. Greiner, C. Regal, and D. Jin, Nature **426**, 537 (2003).
8. W. Zwerger, *The BCS-BEC crossover and the unitary Fermi gas*, vol. 836 (Springer, 2011).
9. M. Fisher, P. Weichman, G. Grinstein, and D. Fisher, Phys. Rev. B **40**, 546 (1989).
10. M. Greiner, O. Mandel, T. Esslinger, T. Hänsch, and I. Bloch, Nature **415**, 39 (2002).
11. R. Jördens, N. Strohmaier, K. Günter, H. Moritz, and T. Esslinger, Nature **455**, 204 (2008).
12. M. Köhl, H. Moritz, T. Stöferle, K. Günter, and T. Esslinger, Physical review letters **94**, 080403 (2005).
13. J. Dalibard, F. Gerbier, G. Juzeliūnas, and P. Öhberg, Reviews of Modern Physics **83**, 1523 (2011).
14. R. Dum and M. Olshanii, Physical review letters **76**, 1788 (1996).
15. Y.-J. Lin, R. Compton, K. Jimenez-Garcia, J. Porto, and I. Spielman, Nature **462**, 628 (2009).
16. H. Miyake, G. Siviloglou, C. Kennedy, W. Burton, and W. Ketterle, Phys. Rev. Lett. **111**, 185302 (2013).
17. M. Aidelsburger, M. Atala, S. Nascimbène, S. Trotzky, Y.-A. Chen, and I. Bloch, Phys. Rev. Lett. **107**, 255301 (2011).
18. M. Aidelsburger, M. Atala, S. Nascimbène, S. Trotzky, Y.-A. Chen, and I. Bloch, Appl. Phys. B **113**, 1 (2013).
19. K. Jimenez-Garcia, L. LeBlanc, R. Williams, M. Beeler, A. Perry, and I. Spielman, Phys. Rev. Lett. **108**, 225303 (2012).
20. J. Struck, C. Ölschläger, M. Weinberg, P. Hauke, J. Simonet, A. Eckardt, M. Lewenstein, K. Sengstock, and P. Windpassinger, Phys. Rev. Lett. **108**, 225304 (2012).
21. J. Struck, M. Weinberg, C. Ölschläger, P. Windpassinger, J. Simonet, K. Sengstock, R. Höppner, P. Hauke, A. Eckardt, M. Lewenstein, et al., Nat. Phys. **9**, 738 (2013).
22. D.R. Hofstadter, Phys. Rev. B **14**, 2239 (1976).
23. Y.-J. Lin, K. Jimenez-Garcia, and I. Spielman, Nature **471**, 83 (2011).
24. P. Wang, Z.-Q. Yu, Z. Fu, J. Miao, L. Huang, S. Chai, H. Zhai, and J. Zhang, Phys. Rev. Lett. **109**, 095301 (2012).
25. L. Cheuk, A. Sommer, Z. Hadzibabic, T. Yefsah, W. Bakr, and M. Zwierlein, Phys. Rev. Lett. **109**, 095302 (2012).
26. C. Kennedy, G. Siviloglou, H. Miyake, W. Burton, and W. Ketterle, Phys. Rev. Lett. **111**, 225301 (2013).
27. M. Aidelsburger, M. Atala, M. Lohse, J. Barreiro, B. Paredes, and I. Bloch, Phys. Rev. Lett. **111**, 185301 (2013).
28. C.L. Kane and E.J. Mele, Phys. Rev. Lett. **95**, 146802 (2005).
29. L. Fu, C. Kane, and E. Mele, Phys. Rev. Lett. **98**, 106803 (2007).
30. R. Roy, Phys. Rev. B **79**, 195322 (2009).
31. M. Beeler, R. Williams, K. Jimenez-Garcia, L. LeBlanc, A. Perry, and I. Spielman, Nature **498**, 201 (2013).
32. L.-K. Lim, C. Smith, and A. Hemmerich, Phys. Rev. Lett. **100**, 130402 (2008).
33. V. Stojanović, C. Wu, W. Liu, and S. Das Sarma, Phys. Rev. Lett. **101**, 125301 (2008).
34. M. Polini, R. Fazio, A. MacDonald, and M. Tosi, Phys. Rev. Lett. **95**, 010401 (2005).
35. G. Wirth, M. Olschlager, and A. Hemmerich, Nat. Phys. **7**, 147 (2011).
36. S. Sinha and K. Sengupta, Europhys. Lett. **93**, 30005 (2011).
37. A. Dhar, M. Maji, T. Mishra, R. Pai, S. Mukerjee, and A. Paramekanti, Phys. Rev. A **85**, 041602 (2012).
38. A. Dhar, T. Mishra, M. Maji, R. Pai, S. Mukerjee, and A. Paramekanti, Phys. Rev. B **87**, 174501 (2013).
39. M. Zaletel, S. Parameswaran, A. Rüegg, and E. Altman, Phys. Rev. B **89**, 155142 (2014).
40. A. Tokuno and A. Georges, ArXiv e-prints (2014), 1403.0413.
41. A. Petrescu and K. Le Hur, Phys. Rev. Lett. **111**, 150601 (2013).
42. S. Teitel and C. Jayaprakash, Phys. Rev. B **27**, 598 (1983).
43. P. Olsson, Phys. Rev. Lett. **75**, 2758 (1995).
44. E. Granato, Phys. Rev. B **48**, 7727 (1993).
45. E. Granato, Journal of Applied Physics **75**, 6960 (1994).
46. P. Olsson, Phys. Rev. Lett. **75**, 2758 (1995).
47. S. White, Phys. Rev. Lett. **69**, 2863 (1992).
48. U. Schollwöck, Rev. Mod. Phys. **77**, 259 (2005).
49. H. Weber and P. Minnhagen, Phys. Rev. B **37**, 5986 (1988).
50. K. Binder and D. Heermann, *Monte Carlo simulation in statistical physics: An introduction* (Springer, 2010).
51. Y. Nishiyama, Eur. Phys. J. B **17**, 295 (2000).

Subroto Mukerjee got his bachelor's degree in Physics from the University of Delhi, master's degree from the Indian Institute of Science in Bangalore and Ph.D. from Princeton University. He has been a postdoctoral fellow at the University of California in Berkeley and is currently an Assistant Professor in the Department of Physics at the Indian Institute of Science. His research is in the in area of theoretical condensed matter physics, specifically the physics of cold atoms, transport in strongly correlated systems and thermalization and quantum information in many-body systems. He is currently a Ramanujan fellow of the Department of Science and Technology, Government of India and has been an Associate of the Indian Academy of Sciences from 2010 to 2013.